Journal of Materials Chemistry C

PAPER

View Article Online
View Journal | View Issue

Cite this: J. Mater. Chem. C, 2015, 3, 8142

A solvent-resistant azide-based hole injection/transporting conjugated polymer for fluorescent and phosphorescent light-emitting diodes†

Cheng-Wei Huang,[a] Feng-Chih Chang,[ab] Yu-Lin Chu,[a] Cheng-Chang Lai,[c] Tzu-En Lin,[a] Chao-Yuan Zhu*[a] and Shiao-Wei Kuo*[b]

Received 17th June 2015,
Accepted 5th July 2015

DOI: 10.1039/c5tc01794g

www.rsc.org/MaterialsC

Interfacial mixing of polymers is a critical issue when attempting to improve the charge transport and stabilize the operation of solution-processed organic light-emitting diodes (OLEDs). Herein, we describe a simple methodology for overcoming interfacial mixing, based on the use of a photo-crosslinkable hole injection/transporting material (HITM). We synthesized a conjugated polymer, PTCAzide, bearing ready crosslinking ability and investigated its suitability for use as an HITM. Photo-crosslinking of the PTCAzide copolymer gave X-PTCAzide, which exhibited much higher thermal stability (the glass transition temperature increased by 21 K relative to that of PTCAzide), remarkable electrochemical stability, and excellent solvent-resistance, thereby expanding the operation time of corresponding electronic devices. Such a tris(8-hydroxyquinolinato)aluminum-based trilayer device reached a maximum brightness of 52 971 cd m^{-2}, and the maximum luminance efficiency (LE) and power efficiency (ηE) are both higher than those of the corresponding device based on commercial PEDOT : PSS. In addition, a solution-processed phosphorescent OLED device incorporating X-PTCAzide also exhibited good performance (external quantum efficiency: 7.93%; LE: 29.6 cd A^{-1}; ηE: 14.3 lm W^{-1}; maximum brightness: 34 484 cd m^{-2}). The efficient and simple photocrosslinking without adding an initiator could facilitate the fabrication process. Thus, PTCAzide appears to be a promising next-generation HITM for the development of highly efficient and inexpensive OLEDs. Its photo-crosslinkable nature allows improvements in morphological stability and hole injection/transporting ability, leading to more stable devices with better operation, without disrupting molecular packing or charge transport.

Introduction

High-performance organic light-emitting devices (OLEDs) are promising systems for display and solid-state lighting applications because of their low power consumption, wide viewing angles, rapid responses, and potential use in light-weight flexible devices.[1] The discovery of conjugated polymers allowed scientists to extend the applicability of organic semiconductors to, for example, electrochromic devices,[2] organic thin-film transistors,[3] photovoltaic cells,[4] and OLEDs,[5] all with the possibility of processing from solution. For OLEDs, multilayer devices are preferred over single-layer devices because of their greater efficiencies. In such devices, charge transport and carrier balance are two factors that can seriously affect the efficiency.[6] To achieve optimal device performance, the polymeric materials must display superior hole injection/transporting behavior with good mechanical properties and thermal stability. The most widely used HITL (hole injection/transporting layer) in OLEDs is poly(3,4-ethylenedioxythiophene) : polystyrenesulfonate (PEDOT : PSS), which possesses high conductivity (*ca.* 1–10 S cm^{-1}), sufficient transparency in the visible region, and good film-forming properties.[7] Nevertheless, there are several drawbacks when using PEDOT : PSS as the HITL, including the need for a water-based fabrication process (the presence of residual water can cause more serious pollution than that provided by oxygen in terms of device degradation),[8] corrosion of the indium tin oxide (ITO) surface,[9] poor hole injection for most blue- and green-emitting materials (due to inadequate energy levels), and exciton quenching at the interface between the PEDOT : PSS film and the emitting layer (EML).[10] Accordingly, superior HITL materials are being actively pursued for use in solution-processed OLEDs.

Interfacial mixing between layers is an inevitable problem in solution-processed multilayer devices, with several approaches having been proposed to overcome it, including the design of orthogonal solubility,[11] the use of precursor polymers,[12]

[a] Institute of Applied Chemistry, National Chiao Tung University, Hsinchu, 30010 Taiwan. E-mail: cyzhu@mail.nctu.edu.tw
[b] Department of Materials and Optoelectronic Science, National Sun Yat-Sen University, Kaohsiung, 804, Taiwan. E-mail: kuosw@faculty.nsysu.edu.tw
[c] Department of Chemistry, National Tsing Hua University, Hsinchu, 30013, Taiwan
† Electronic supplementary information (ESI) available. See DOI: 10.1039/c5tc01794g

and the application of a variety of cross-linked materials. There has recently been a huge effort to develop cross-linking strategies to enhance solvent-resistance.[13] Several chemical cross-linking methods have been reported based on heat-treatment,[14,15] cross-linking reagents,[16] and functionalized cross-linkable units.[17] To maintain the film morphology and minimize production costs, a suitable processing temperature (<120 °C, preferably) should be considered when designing OLED materials. This request has limited the applications of thermally crosslinkable hole injection/transporting materials (HITMs). Unfortunately, even though the concept may be useful, the introduction of cross-linking functional groups to conjugated polymers often worsens the device performance, due to their effect on disturbing molecular packing.[18] Moreover, some of the approaches mentioned above may require relatively high fabrication temperatures, limiting their industrial applicability. Thus, there remain several challenges in the development of better cross-linkable HITMs for high-performance OLEDs.

In a previous study, we found that a HITM featuring an arylamine backbone led to a remarkable enhancement in the efficiency of a corresponding tris(8-hydroxyquinolinato) aluminum (Alq_3)-based fluorescent OLED.[19] The side chain-induced network structure can assist in improving electronic communication between conjugated main chains, thereby increasing hole mobility.[21] For further application in solution-processed phosphorescent OLEDs, good solvent-resistance is required to overcome the problem of interfacial mixing. Azide-induced crosslinking is a powerful strategy for improving solvent-resistance and thermal stability. Azide units can be photo-crosslinked readily under deep-ultraviolet illumination (DUV, 254 nm) while maintaining the original electrochemical properties of the conjugated system.[22,23] Organic azides have been used as a crosslinking reagent to induce covalent crosslinking, including biomedical application.[24] However, to the best of our knowledge, only a few research studies use azide as a crosslinking protocol for fabricating electronic devices. In this study, we developed a readily synthesized azide-containing conjugated copolymer, PTCAzide, through Suzuki polycondensation. The alkyl chain spacers presented azide units that provided the possibility of photo-crosslinking while also modulating the electrical response.[19] To investigate the ability of such polymers to function as HITMs, we fabricated Alq_3-based trilayer OLED devices incorporating them, achieving a luminance efficiency (LE) of 8.5 cd A^{-1} and a maximum brightness of 52 971 cd m^{-2}—both values are higher than those of devices based on commercial PEDOT : PSS. The photo-crosslinkable azide moieties allowed us to produce a solvent-resistant HITM for use in OLEDs. Therefore, we fabricated solution-processed phosphorescent OLED devices with PTCAzide and X-PTCAzide (material after crosslinking). The device incorporating X-PTCAzide exhibited performance [external quantum efficiency (EQE): 7.93%; LE: 29.6 cd A^{-1}; ηE: 14.3 lm W^{-1}; maximum brightness: 34 484 cd m^{-2}] superior to that of devices based on PTCAzide and PEDOT : PSS. Thus, it is possible to fabricate efficient OLEDs using our materials through a simple and efficient crosslinking process, the resulting HITL could overcome the problem of interfacial mixing and decreases the cost of fabrication.

Experimental section

Materials

All solvents were purchased from TEDIA (USA) and distilled over CaH_2 prior to use. Commercially available reagents were obtained from Sigma-Aldrich or Acros and were used as received. 4-Butyl-*N*,*N*-bis(4-bromophenyl)aniline (**1**, Fig. S1, ESI†), 4-butyl-*N*,*N*-bis-(4,4,5,5-tetramethyl-1,3,2-dioxaborolane-4-phenyl)aniline (**2**, Fig. S1 and S2, ESI†), and 3,6-dibromocarbazole (**3**, Fig. S3, ESI†) were synthesized according to previously reported processes.[19] 6-Bromobutyl-9(3,6-carbazole) (**4**, Fig. S1, ESI†) was prepared according to the literature.[20]

6-Azidohexyl-9(3,6-carbazole) (5)

Sodium azide (NaN_3; 0.85 g, 13.1 mmol), powdered ammonium chloride (NH_4Cl; 0.35 g, 6.51 mmol), and 6-bromobutyl-9-(3,6-carbazole) (**4**; 2.13 g, 4.36 mmol) were dissolved in dry DMF in a reaction flask fitted with a condenser. After purging under argon, the mixture was heated and stirred overnight at 85 °C. The mixture was cooled, filtered and concentrated under vacuum to remove the solvent. EtOAc (150 mL) was added and then the organic phase was extracted with distilled water (3×150 mL). The organic phase was dried ($MgSO_4$), filtered, and concentrated. The residue was purified through column chromatography [SiO_2; EtOAc/hexane, 1 : 10 (v/v)] to give a white powder (1.8 g, 92%). ^{1}H NMR (Fig. S3, ESI,† $CDCl_3$, δ): 8.10 (d, 2H; ArH), 7.54 (dd, 2H; ArH), 7.25 (d, 2H; ArH), 4.25 (t, 2H; CH_2), 3.20 (t, 2H; CH_2N_3), 1.84 (m, 2H; CH_2), 1.53–1.36 (m, 6H; CH_2). ^{13}C NMR (Fig. S4, ESI,† $CDCl_3$, δ): 140.0, 129.7, 124.1, 123.6, 112.7, 110.7, 51.9, 43.4, 28.9, 28.8, 26.9, 26.6.

PTCAzide

A deoxygenated mixture of THF (4 mL) and 2 M aqueous K_2CO_3 (2.7 mL) were added to a mixture of **2** (0.413 g, 0.644 mmol), **5** (0.290 g, 0.644 mmol), several drops of Aliquat 336®, and freshly prepared $Pd(0)(PPh_3)_4$ (0.015 g, 12.9 mmol). The mixture was heated at 65 °C with stirring for 96 h, and then slowly poured into a mixture of MeOH/deionized water (10 : 1, v/v). The precipitated polymer was collected and purified by redissolving in chloroform and precipitating several times from acetone to remove any oligomers and catalyst residues. The resulting solid was dried under high vacuum to yield a light-brown solid. (Yield: 70%) ^{1}H NMR (Fig. 1, $CDCl_3$, δ): 8.36 (br, ArCH), 7.67 (br, ArCH), 7.06 (br, ArCH), 4.34 (br, NCH_2), 3.23 (br, CH_2N_3), 2.6 (br, CH_2), 1.92 (br, CH_2), 1.59 (br, CH_2), 1.41 (br, CH_2), 0.96 (t, CH_3).

Light-emitting devices: fabrication and measurements

Patterned ITO-coated glass (sheet resistance: 25 Ω square^{-1}) was washed with detergent, distilled water, and acetone and then immersed in an ultrasonic bath. After removal and drying with a spray gun, the clean ITO glass was exposed to oxygen plasma for 20 min. Solutions of the polymers in 1,1,2,2-tetrachloroethane were filtered through a 0.45 μm PTFE syringe filter and then spin-coated onto the ITO substrate, which was subsequently dried in a vacuum oven at 100 °C for 1 h.

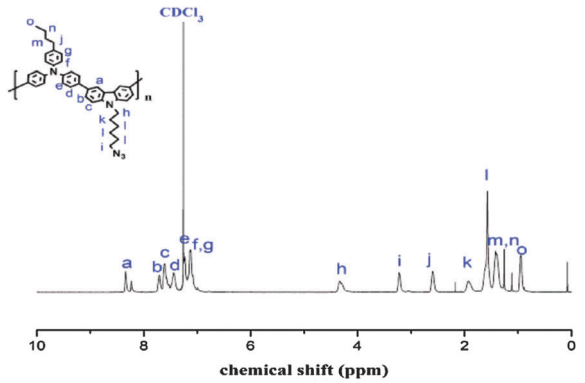

Fig. 1 ^{1}H NMR spectrum of the copolymer PTCAzide.

The organic layers were deposited onto ITO glass at 10^{-6} Torr at a deposition rate of 1.0 Å s^{-1}. Deposition of LiF was accomplished through thermal evaporation at a rate of 0.1 Å s^{-1}. The device was then capped with Al metal at a deposition rate of 4.0 Å s^{-1}. A Newport 1835C optical meter equipped with an 818ST silicon photodiode and a Keithley 2400 source meter were employed to determine the relationship between the current density (or brightness) and the applied voltage. Electroluminescence spectra were recorded using a Hitachi F4500 luminescence spectrometer. The polymer film thickness was determined using an Alfa step 500 surface profiler (Tencor) to be approximately 15 nm.

Characterization

FTIR spectra were measured using a Nicolet Avatar 320 FT-IR spectrometer; 32 scans were collected at room temperature at a resolution of 1 cm^{-1}. Specimens were prepared using the regular KBr disk method with $CHCl_3$ as the casting solvent. ^{1}H and ^{13}C NMR spectra were recorded for samples in deuterated solvent using a Varian UNITY INOVA 500 MHz spectrometer (equipped with a 11.75 T Bruker magnet) at 500 and 125 MHz, respectively. Molecular weights were measured using a Waters 410 GPC system equipped with a refractive index detector and three Ultrastyragel columns (100, 500, and 1000 Å) connected in series. THF was the eluent at a flow rate of 1.0 mL min^{-1} at 25 °C, and the system was calibrated using polystyrene (PS) standards. Differential scanning calorimetry (DSC) was performed using a TA Instruments Q-20 apparatus under an atmosphere of dry N_2. Samples were weighed (3–5 mg) and sealed in an aluminum pan, then scanned from 0 to 200 °C at a rate of 10 K min^{-1}. AFM micrographs were recorded at 20 °C in air using a Dimension 3100 apparatus (Digital Instrument), operated in the tapping regime mode, equipped with silicon cantilever tips (PPP-NCH-50, 204–497 kHz, 10–130 N m^{-1}); and the scan rate was 256 samples $line^{-1}$. UV-Vis spectra were recorded using an HP 8453 diode-array spectrophotometer. Cyclic voltammetry (CV) was performed using a BAS 100 B/W electrochemical analyzer operated at a scan rate of 100 mV s^{-1}. The CV spectrum was recorded under thin film conditions on ITO substrates and used as the working electrode. The potentials were measured against a Ag/Ag^{+} (0.01 M $AgNO_3$) reference electrode with ferrocene/ferrocenium (Fc/Fc^{+}) as an internal standard. For cross-linking experiments, polymer thin films were prepared on ITO substrates through spin-coating (1500 rpm, 1 wt% in $CHCl_3$), followed by photo-crosslinking under a N_2 atmosphere (low-power hand-held UV lamp: 1.9 mW, 254 nm).

Results and discussion

Because of their efficient hole-transporting ability and ready cross-linking, we introduced azide units into the carbazole moieties **5** and copolymerized them with the triphenylamine monomer **2** through Suzuki cross-coupling to form PTCAzide, a photo-crosslinkable HITM. Scheme 1 summarizes the syntheses of the polymer and the corresponding monomers. The conversion from halide to azide is simple and efficient, recovered in 92% yield. After the five-step synthesis, we obtained PTCAzide in a yield of 70%. ^{1}H NMR spectroscopy (Fig. 1) confirmed its structure. The mole percent of azide-functionalized carbazole units was calculated from the integrated areas of peaks *h* and *j*. We observed a value of approximately 50% in the PTCAzide copolymer, consistent with an alternative random copolymer.

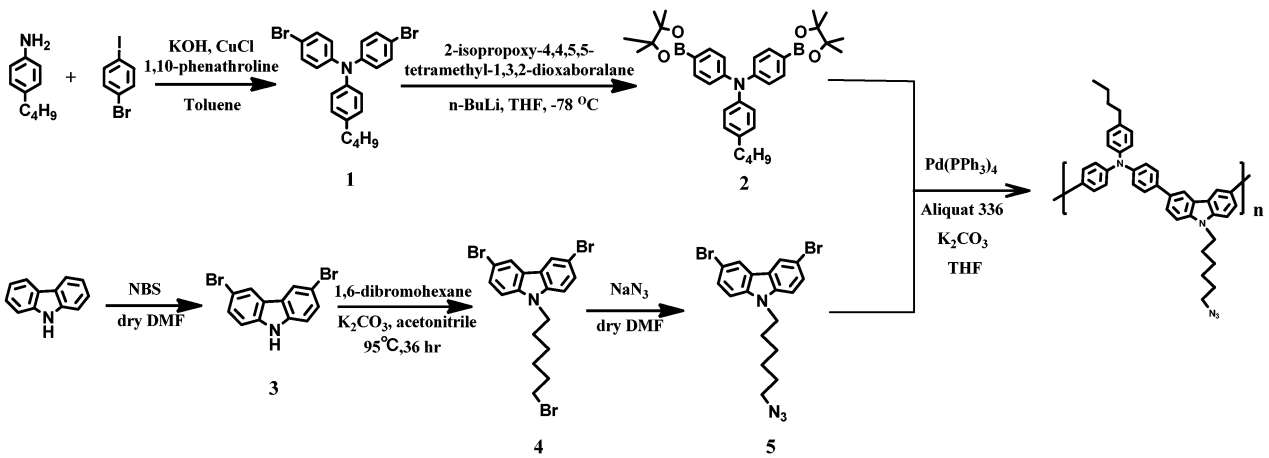

Scheme 1 Synthesis of the cross-linkable conjugated copolymer PTCAzide.

Table 1 Electrochemical properties of HITMs

HITM	$E_{ox,onset}$ [a] [eV]	HOMO [b] [eV]	LUMO [c] [eV]	E_g [d] [eV]
PTCAzide [c]	0.40	−5.20	−2.20	3.00
X-PTCAzide [b]	0.33	−5.13	−2.14	2.99

[a] Values of $E_{ox,onset}$ were measured through CV using ferrocene as the internal standard. [b] HOMO = $E_{ox,onset}$ + 4.8 eV. [c] LUMO = HOMO − E_g. [d] Values of E_g were obtained from UV-Vis absorption spectra (film).

Fig. S5 (ESI†) provides molecular weight information for PTCAzide (M_n = 4600; M_w = 8250; PDI = 1.80). The degree of polymerization is *ca.* 8. FTIR spectroscopy was used to confirm the chemical structures of the monomers and polymers. The existence of a signal for azide stretching (2098 cm^{-1}; Fig. S6, ESI†) indicated that the photo-crosslinkable azide functionalities have been introduced into the conjugated polymer. Table 1 summarizes the electrochemical properties of PTCAzide. This novel photo-crosslinkable HITM exhibited good solubility in common organic solvents (THF, toluene, dichloromethane, chlorobenzene), allowing ready processing during OLED device fabrication.

Furthermore, because the crosslinking mechanism is non-specific (does not require two particular groups to bond together), we expected high photocrosslinking efficiency. To characterize the cross-linking ability, we prepared polymer thin films on KBr disks and followed their photo-crosslinking processes under a N_2 atmosphere. Fig. 2 reveals that the intensity of the peak at 2098 cm^{-1} decreased upon increasing the illumination time, finally disappearing after 1 h—consistent with a cross-linking reaction occurring in the polymer films. In addition, the thin films after illumination were completely insoluble in common organic solvents, suggesting that they had been cross-linked through this simple photo-crosslinking process (Fig. S7, ESI†). After chlorobenzene rinsing the PTCAzide film was partially dissolved and caused strong fluorescent solution. In contrast, X-PTCAzide showed no effect on the solution. The cross-linked thin films also exhibited high transparency, absorbing mainly in the UV region, potentially minimizing interference when emitting light from the device.

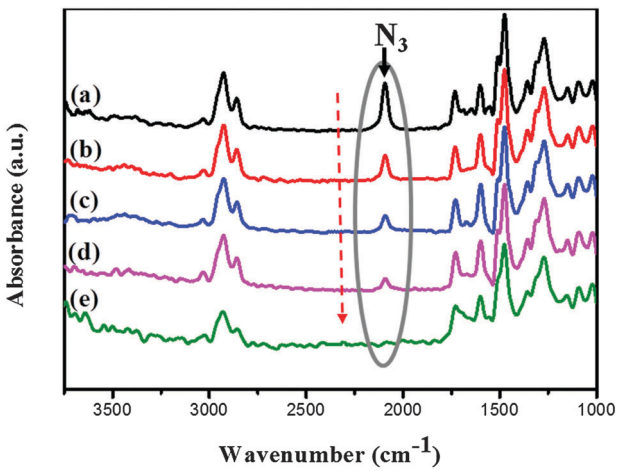

Fig. 2 FTIR spectra of PTCAzide (a) before and (b–d) after UV illumination for (b) 10 min, (c) 20 min, (d) 40 min, and (e) 1 h.

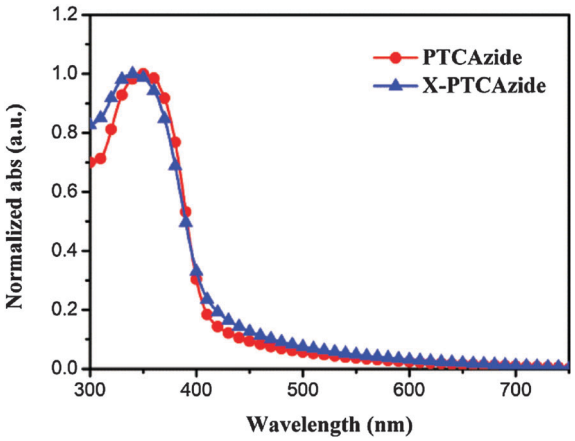

Fig. 3 Normalized UV-Vis absorption spectra of PTCAzide and X-PTCAzide.

To gain deeper insight into the photophysical properties of the cross-linkable HTM, we measured its UV-Vis absorption. Fig. 3 reveals that the absorption maximum of PTCAzide appears near 352 nm, attributable to the π–π* transition of the conjugated arylamine functionality. PTCAzide did not absorb in the emission range of common organic emitters, potentially minimizing the risk of polymer photo-oxidation. No shoulder peaks were evident in the UV-Vis spectra, consistent with the reported polymer having conjugated units only in its main chain. When we crosslinked PTCAzide upon DUV irradiation, its color turned from yellow to light-orange. Similar chromic phenomena have been observed for other non-regioregular conjugated polymers,[25] suggesting a change in polymer conformation and conjugation length. After crosslinking, the absorption signal of the polymer film shifted slightly to 340 nm. Such a blue-shift generally indicates a shortening of the conjugation length along a polymer backbone, mainly through a conformational change or an interruption in conjugation caused by the insertion of nitrenes. Nevertheless, the peak shift for our material was small, meaning that any disruption in conjugation was not very severe. During photolysis, the decomposition of azide units generates reactive nitrenes that can react with neighboring molecules, leading to crosslinking and the formation of insoluble polymer films.[26] This crosslinking strategy can enhance the thermal properties of materials. Fig. 4(a) presents the DSC analysis of PTCAzide and a clear glass transition temperature (T_g) was evident at 109.4 °C during the second heating cycle. After photo-crosslinking, we found a higher value of T_g [130.6 °C, Fig. 4(b)], consistent with the generation of a completely solvent-resistant crosslinked network. Moreover, no melting or crystallization peaks were evident during the DSC heating and cooling process for these two materials, suggesting that both were highly amorphous—presumably because of poor packing of the alternating copolymer of triphenylamine and 3,6-carbazole moieties, consistent with previous reports.[19,27] The increased value of T_g and the amorphous nature of such polymer films suggest that they could maintain long-term morphological stability with suppressed crystallization and aggregation.

We used this new hole transporting material PTCAzide with a crosslinkable azide functionality to avoid the problem of

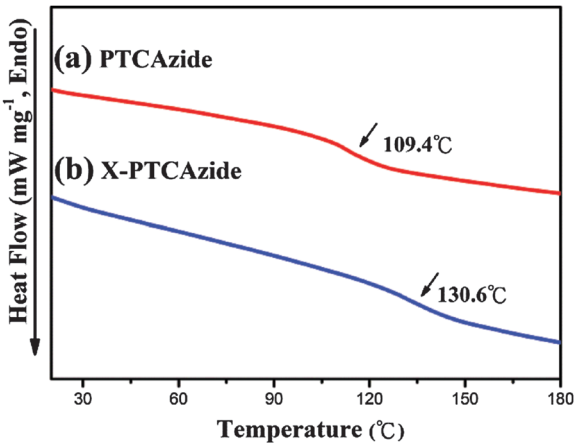

Fig. 4 DSC thermograms of (a) PTCAzide and (b) X-PTCAzide.

interfacial mixing during the multilayer OLED fabrication in solution. To further test its solvent-resistance, the UV-Vis absorption spectrum of polymer thin films was recorded before and after rinsing with chlorobenzene, a common spin-coating solvent used for deposition of the emissive layer in PHOLEDs. Fig. 5 reveals that the absorption of pristine PTCAzide disappeared 55% after rinsing with chlorobenzene, confirming that the polymer film had high solubility in chlorobenzene and dissolved during the rinsing process. In other words, a thin film of pristine PTCAzide would not have enough solvent-resistance against chlorobenzene. In contrast, we generated a robust film of X-PTCAzide after photo-crosslinking, as evidenced by the absence of any change in its absorption intensity after rinsing. Thus, the crosslinked structure of X-PTCAzide provided strong solvent-resistance against chlorobenzene. Therefore, the solution-processability and strong solvent-resistance of X-PTCAzide appeared beneficial for the fabrication of multilayer OLEDs.

We used CV to investigate the electrochemical characteristics of PTCAzide and X-PTCAzide. Pure PTCAzide exhibited relatively poor electrochemical stability and degraded significantly upon repeated scanning [Fig. 6(a)], indicating that the azide-induced

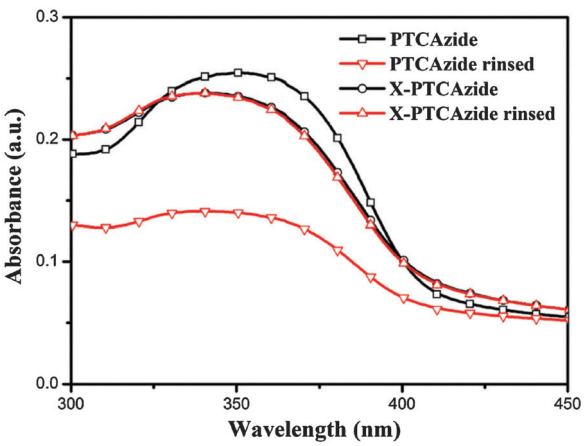

Fig. 5 UV-Vis absorption spectra of pristine PTCAzide and X-PTCAzide before and after rinsing with chlorobenzene.

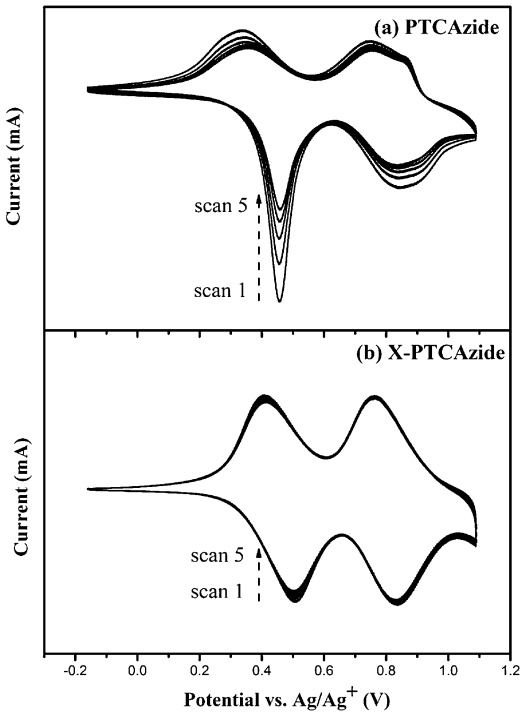

Fig. 6 Cyclic voltammograms of (a) PTCAzide and (b) X-PTCAzide on ITO substrates scanned three times at a scan rate of 100 mV s^{-1}.

photo-crosslinking was important to enhance the robustness and electrochemical stability of HITL. For X-PTCAzide, however, two oxidative peaks were clearly distinguishable at anodic peak potentials (E_{pa}) of 0.51 and 0.84 V (Fig. S8, ESI†). The first oxidation peak appears to involve the electron loss process from the electron-rich triphenylamine unit in the conjugated polymer backbone. The second oxidation peak was contributed to the carbazole moiety. As shown in Fig. S9 (ESI†), during the scanning process the current gradually decreases. This result may be caused by the poor solvent-resistance of PTCAzide against acetonitrile. In contrast, X-PTCAzide preserved good electrochemical activity after repeated scans, which might result from good solvent-resistance, stability of the film and good adhesion to the ITO substrate. After repeated scans (>10 cycle), the voltammogram of PTCAzide become similar to X-PTCAzide ($I_{pa}/I_{pc} \sim 1$) and the robustness was enhanced. This result suggested that PTCAzide can not only crosslink upon UV illumination but also by an electrochemical process. The CV curve revealed fully reversible electrochemical behavior [Fig. 6(b)] and essentially unchanged cathodic and anodic peak currents during repeated scanning, indicating that X-PTCAzide had excellent electrochemical stability.

To assess the charge injection ability of the polymer, we measured the electrochemical characteristics (Table 1). The estimated energy levels of the highest occupied molecular orbital (HOMO) and the lowest unoccupied molecular orbital (LUMO) of X-PTCAzide are −5.13 and −2.14 eV, respectively, as determined from the CV traces and the optical band gap (measured from the absorption spectra). We also calculated the HOMO and LUMO energy levels of PTCAzide in the same way, prior to crosslinking

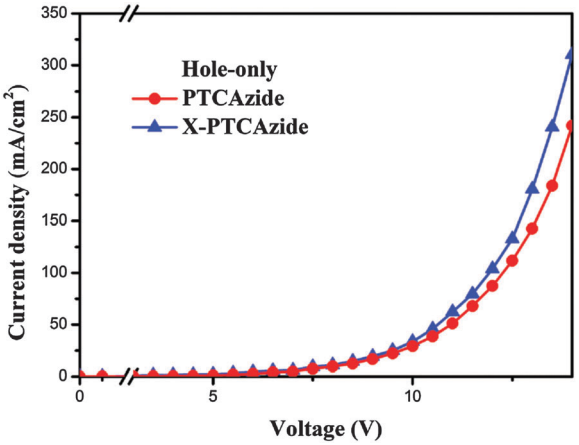

Fig. 7 *I*–*V* characteristic of hole-only devices [ITO/HITL (15 nm)/NPB/Al].

of the film. The HOMO energy level of X-PTCAzide is very close to the work function of ITO glass (−4.9 eV), suggesting a barrier height (ΔE_h) for hole injection between ITO and X-PTCAzide of only 0.2 eV, potentially facilitating the injection/transport of holes and further improving the performance of OLEDs.

To investigate the hole-transporting properties of HITMs, we fabricated hole-only devices with the structure ITO/HITL (15 nm)/NPB/Al, incorporating PTCAzide before and after crosslinking. A remarkable decrease in performance is usually observed when incorporating triarylamine-based photo-crosslinking materials, due to partial photodecomposition and a decreased mobility of triarylamine units.[25] The current density of X-PTCAzide, however, exhibited only a slight change compared with that of the polymer deposited without crosslinking (Fig. 7). Furthermore, the current maximum of the crosslinked hole-only device increased to a value larger than that of the non-crosslinked device, consistent with earlier findings for other functionalized photo-crosslinkable materials.[28,29] The higher current maximum may have caused by the greater morphological stability and stronger electrochemical properties under high operating voltage. Thus, the formation of a cross-linked network increased the current maximum while only slightly disrupting hole transport ability. Accordingly, we expected improved device performance when using X-PTCAzide as the HITL.

Performance of fluorescent OLEDs

To determine whether cross-linked X-PTCAzide would serve as an effective HITL, we fabricated a fluorescent-type OLED device having the device structure ITO/HITL (15 nm)/NPB (15 nm)/Alq_3 (60 nm)/LiF (1 nm)/Al (100 nm) [Fig. 8(d)]. The EL spectrum of the device peaked at 520 nm (Fig. S10, ESI†), and the signal

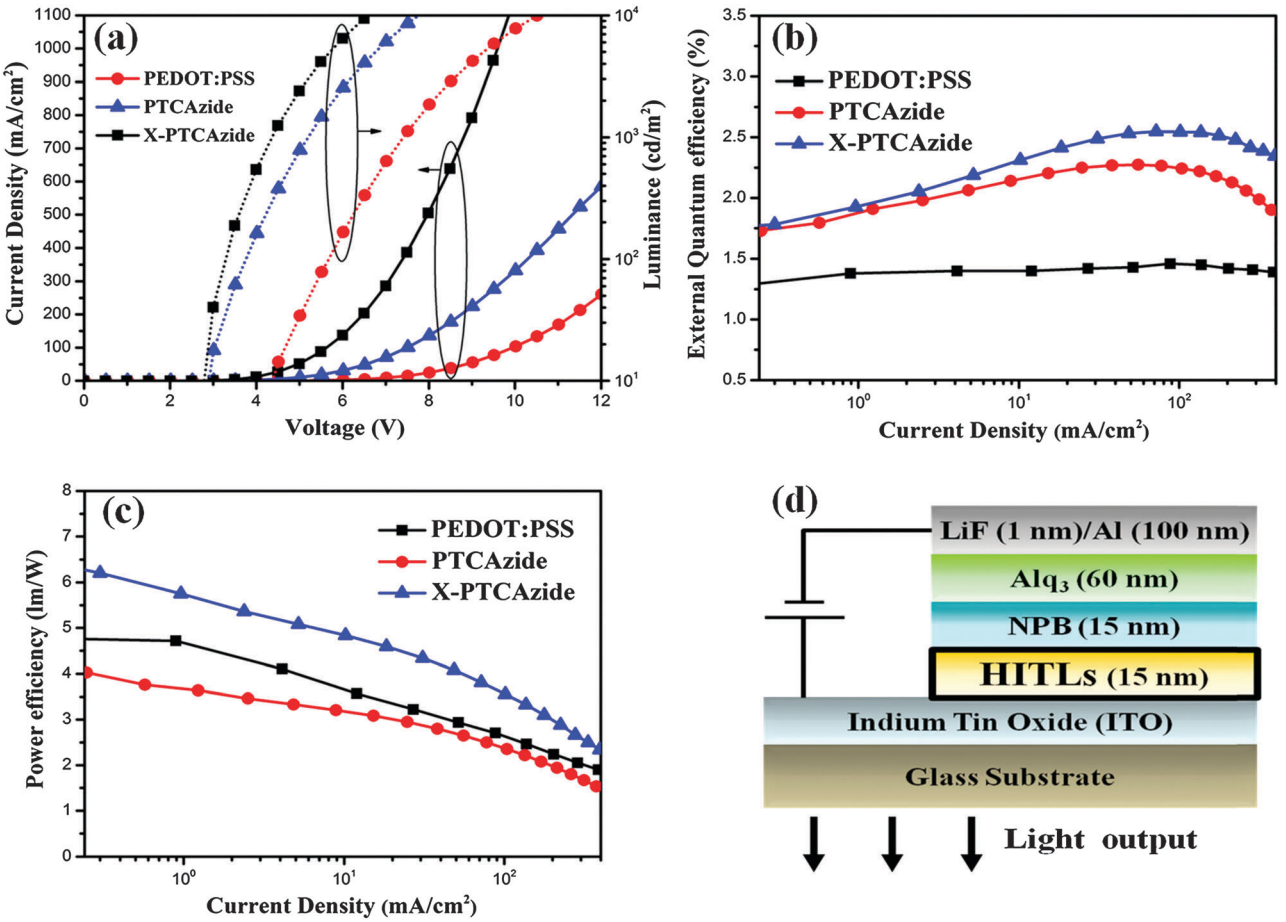

Fig. 8 (a) *I*–*V*–*L*, (b) EQE–*I*, and (c) ηE–*I* characteristics; (d) schematic representation of the ITO/HITL/NPB/Alq_3/LiF/Al devices.

Table 2 Electroluminescence devices having the structure ITO/HITL/NPB/Alq_3/LiF/Al [**1**] and ITO/HITLs/$Ir(ppy)_3$: PVK/BCP/Alq_3/LiF/Al [**2**]

(a)

HITL [**1**]	V_{on}[d] [V]	Q_{max}[e] [%]	LE_{max}[f] [cd A^{-1}]	ηE_{max}[g] [lm W^{-1}]	B_{max}[h] [cd m^{-2}]	EQE_{1000}[i] [%]	LE_{1000}[j] [cd m^{-2}]
PEDOT : PSS[a]	2.4	1.46	4.7	3.57	41 948	1.41	4.53
PTCAzide[b]	3.1	2.27	7.6	4.03	31 774	2.19	7.31
X-PTCAzide[c]	2.4	2.55	8.5	4.8	52 971	2.34	7.83

(b)

HITL [**2**]	V_{on}[d] [V]	Q_{max}[e] [%]	LE_{max}[f] [cd A^{-1}]	ηE_{max}[g] [lm W^{-1}]	B_{max}[h] [cd m^{-2}]	EQE_{1000}[i] [%]	LE_{1000}[j] [cd m^{-2}]
PEDOT : PSS[a]	4.1	6.66	25.1	12.9	29 321	6.4	24.1
PTCAzide[b]	4.1	6.57	24.7	10.4	27 089	6.4	16.0
X-PTCAzide[c]	4.4	7.93	29.6	14.3	34 484	7.4	25.9

[a] 15 nm. [b] 15 nm. [c] 15 nm, crosslinked upon UV illumination (365 nm, 1 mW cm^{-2}) for 1 h. [d] Turn-on voltage. [e] Maximum external quantum efficiency. [f] Maximum luminance efficiency. [g] Maximum power efficiency. [h] Maximum brightness. [i] EQE at 1000 cd m^{-2}. [j] Luminance efficiency at 1000 cd m^{-2}.

originated from the Alq_3 layer, indicating that the HITM played the role only of a hole-transporting material without any emission caused by exciplex formation with Alq_3. The slight shift of PTCAzide EL spectra was due to the recombination zone drifting effect due to different electrochemical properties of PTCAzide and X-PTCAzide (different HOMO and LUMO value). It affected hole injection/transporting properties thereby causing the red shift of EL spectra. Fig. 8(a) and Table 2(a) display the current density–voltage–luminance (*I–V–L*) characteristics of these green-light-emitting devices. In addition to a lower turn-on voltage (2.4 V, obtained at 1 cd m^{-2}), the device based on X-PTCAzide also exhibited an operating voltage substantially lower than that of the PTCAzide-based device at the same current density. The *L–V* properties of the devices revealed that the luminance of the X-PTCAzide-based device was higher than that of the PTCAzide-based device over the entire range of voltages. Fig. 8(b) and (c) display the EQEs and power efficiencies (ηE) plotted with respect to the current density. (As listed in Table 2, the LE of the PTCAzide-based device (7.6 cd A^{-1}) and X-PTCAzide-based device (8.5 cd A^{-1}) are both higher than those of a corresponding device based on commercial PEDOT : PSS.)[19] The power efficiency (ηE) curves of the two materials were similar. The device based on X-PTCAzide exhibited extremely high maximum brightness (52 971 cd m^{-2}), substantially greater than those of the devices based on PEDOT : PSS and PTCAzide. It may have been caused by the robust structure formed by the crosslinked conjugated polymer, improving the sustainability under the high operating voltage and, thus, increasing the maximum brightness. Furthermore, the HOMO energy levels of PTCAzide (−5.20 eV) and X-PTCAzide (−5.13 eV) are suitable for hole injection/transport, making them suitable materials for OLED fabrication.

Fig. S12 (ESI†) shows the plots of relative brightness L/L_0 *vs.* time for these four devices operated at a constant current density. Both of these devices exhibit initial brightness at 1000 cd cm^{-2}. As shown in Fig. S12 (ESI†), the device with PTCAzide decayed seriously (~20%) within first operation hour, with a operational lifetime (T_{70}) of 6 h. Compared with PTCAzide, the X-PTCAzide device did not show any sudden decrease during measurement. The T_{70} of X-PTCAzide is estimated to be 17 h, which is approximately 3 times that of PTCAzide. The reason for the longer lifetime of the X-PTCAzide device could be due to the higher glass transition temperature (T_g) of X-PTCAzide, balanced charge injection and good electrochemical stability compared with PTCAzide. The operational stability results suggest that the crosslinking method we introduced can thus enhance the durability of the entire device.

Surface smoothness is a critical factor affecting the adhesion between various layers. Single-component HTM films usually suffer from significant phase-segregation. Even for cross-linked blends, some degree of segregation is typically observed.[30] Fig. 9 displays AFM images of the devices incorporating PTCAzide and X-PTCAzide. We observe very smooth, uniform surfaces with no obvious pinholes or cracks; the surfaces of the PTCAzide- and X-PTCAzide-covered ITO had a root-mean-square (rms) roughnesses of 0.75 and 0.81 nm, respectively. Both were much smoother than the ITO substrate (3.0–3.7 nm, as reported),[31] indicating that our HITMs remained stable even after treatment at a temperature of 100 °C. The amorphous nature also avoided the effects of phase segregation and crystallization during the operation of the devices. Nevertheless, the PTCAzide-based device displayed an apparently cloudy surface in the emitting

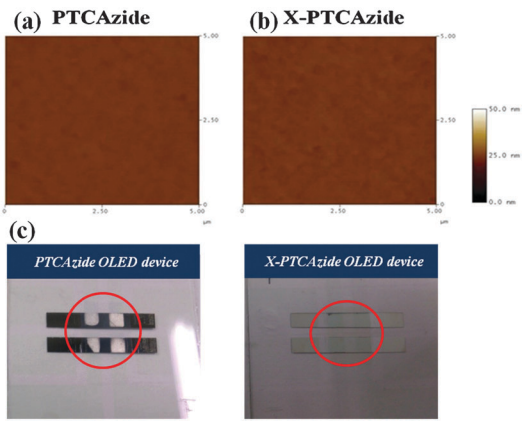

Fig. 9 AFM surface morphologies (tapping mode) of (a) PTCAzide and (b) X-PTCAzide films coated on ITO glass and (c) photographs of PTCAzide and X-PTCAzide devices after operation at 20 V in air.

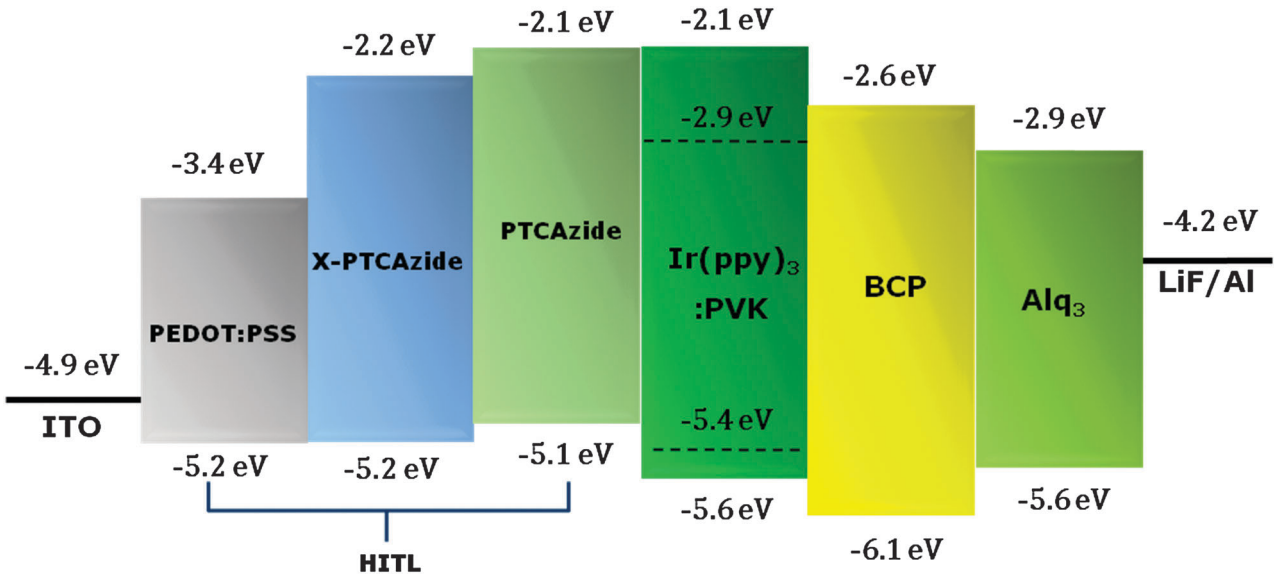

Fig. 10 Corresponding energy level diagrams for the device structures ITO/HITL (PTCAzide, X-PTCAzide, PEDOT : PSS)/Ir(ppy)$_3$: PVK/BCP/Alq$_3$/LiF/Al.

region after measurement [Fig. 9(c)], possibly caused by poor stability under the high operating voltage, which led to the decomposition of the thin organic film and ultimately resulted in oxidation of the whole device. Compared with PTCAzide, X-PTCAzide displayed excellent thermal and electrical stability, which protected the whole device structure from oxidation

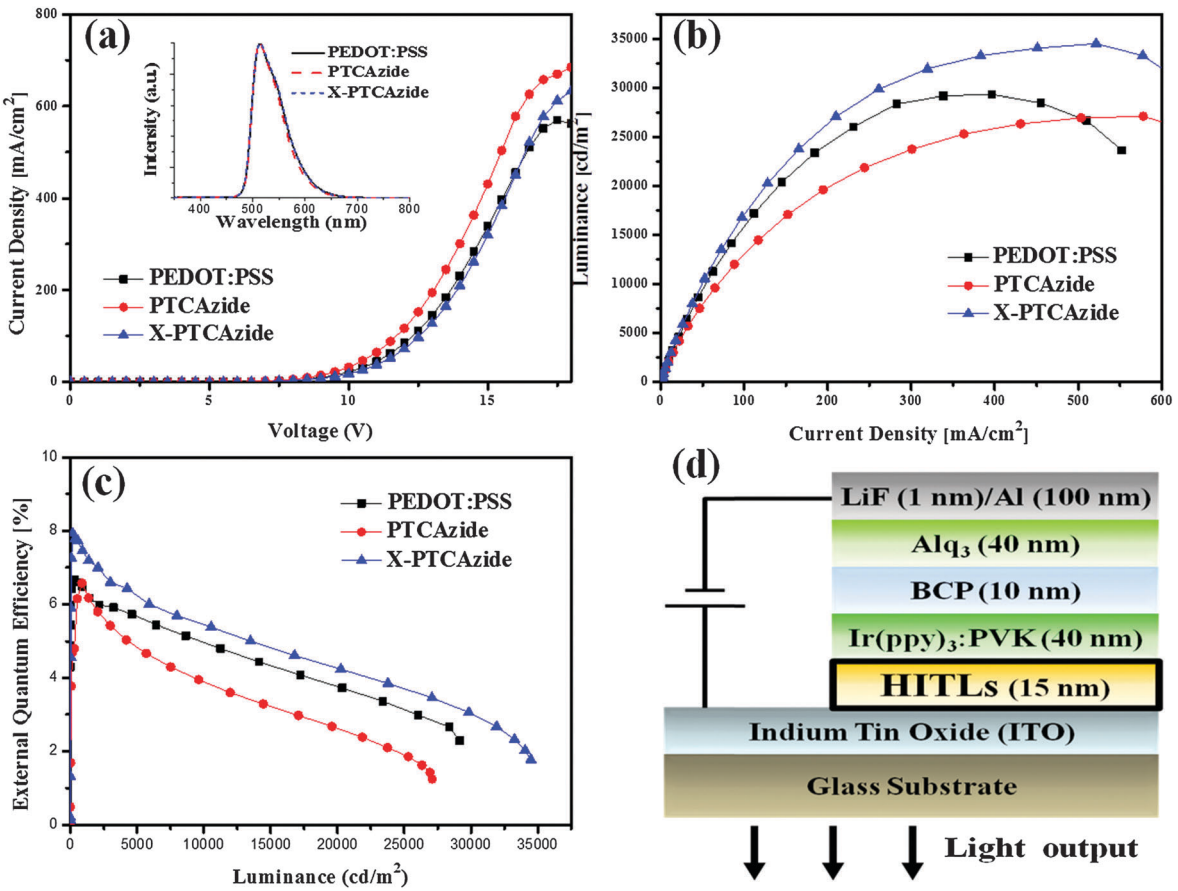

Fig. 11 (a) *I*–*V* (inset: EL spectra), (b) *L*–*I*, and (c) EQE–*I* characteristics; (d) schematic representation of the ITO/HITL (PTCAzide, X-PTCAzide, PEDOT : PSS)/Ir(ppy)$_3$: PVK/BCP/Alq$_3$/LiF/Al devices.

during high-voltage operation, even in air, suggesting that our materials provide other functions: smoothing the rough surface of ITO and enhancing the device stability in air, potentially improving the life times and efficiencies of entire OLED devices.

Performance of solution-processed phosphorescent OLEDs

To evaluate the suitability of X-PTCAzide as an efficient HITL, we fabricated a solution-processed phosphorescent OLED having a device configuration of ITO/HITL/6 wt% *fac*-tris(2-phenylpyridine)-iridium(III) [Ir(ppy)$_3$]: poly(vinyl carbazole) (PVK)/2,9-dimethyl-4,7-diphenyl-1,10-phenanthroline (BCP)/tris(8-hydroxyquinolinato)-aluminum (Alq_3)/LiF/Al, as displayed in Fig. 11(d). Fig. 10 presents the corresponding energy level diagram of the materials used to construct this device.[32] Fig. 11, Fig. S11 (ESI†) and Table 2(b) summarize the display characteristics. As revealed in Fig. 11(c), even PTCAzide exhibited a higher current density than X-PTCAzide, the corresponding device performance was obviously inferior; moreover, we observed (Fig. S13, ESI†) a higher leakage current and a lower turn-on voltage (4.1 V). This behavior was possibly due to the thinner PTCAzide layer obtained after spin-coating the emissive layer on top of it (*i.e.*, because of its poor solvent-resistance, the PTCAzide thin film may have dissolved partially during the process of depositing the emissive layer). In comparison, the excellent solvent-resistance of X-PTCAzide would have ensured no change in its thickness. Table 2(b) reveals that the performance of the device based on X-PTCAzide—a maximum EQE of 7.93%, a maximum LE of 29.6 cd A^{-1}, a maximum power efficiency (ηE) of 14.3 lm W^{-1}, and a maximum brightness of 34 484 cd m^{-2}—was superior to that of the devices incorporating PEDOT: PSS or PTCAzide as the HITL. Under practical conditions of 1000 cd m^{-2}, the LE and EQE were 25.9 cd A^{-1} and 7.4% for the X-PTCAzide-based device, compared with 24.1 cd A^{-1} and 6.4%, respectively, for the PEDOT: PSS-based device. Such excellent performance suggests that X-PTCAzide is a promising material for robust and efficient HITMs for low-cost, solution-processed OLEDs.

Conclusions

We have developed a simple strategy for the preparation of a solvent-resistant HITM using a new amorphous conjugated polymer (PTCAzide) bearing photo-crosslinkable units. The good solubility of PTCAzide in common organic solvents makes it easy to process for applications in organic electronics. Furthermore, the organic thin film obtained after photo-crosslinking (X-PTCAzide) possessed an extremely smooth surface and a robust crosslinked network, without the disruption of the hole injection/transporting properties of PTCAzide, thereby overcoming the problem of interfacial mixing during subsequent solution-processing of the emissive materials. X-PTCAzide also exhibited good electrochemical stability, an enhanced glass transition temperature, and excellent solvent-resistance. The resulting Alq_3-based trilayer device reached a maximum brightness of 52 971 cd m^{-2} and a maximum LE and a power efficiency of 8.5 cd A^{-1} and 4.8 lm W^{-1}, respectively—higher than the values of a device based on commercial PEDOT: PSS. In addition, the performance of solution-processed phosphorescent OLED devices fabricated using X-PTCAzide was also superior to that of devices incorporating PEDOT-PSS. The extraordinarily high hole-injection/transporting capacity results in PTCAzide exhibiting good performance as an HITM, while allowing the possibility to fabricate solution-processed LED devices. Therefore, PTCAzide is a promising next-generation HITM for highly efficient LED devices prepared using low-cost fabrication processes.

Acknowledgements

This study was supported financially by the National Science Council, Taiwan, Republic of China, under contracts MOST103-2221-E-110-079-MY3 and MOST102-2221-E-110-008-MY3. We thank Professor C.-H. Cheng of National Tsing-Hua University for his support and assistance during the preparation and characterization of the LEDs.

References

1 (*a*) S. R. Forrest, *Nature*, 2004, **428**, 911; (*b*) F. So, J. Kido and P. Burrows, *MRS Bull.*, 2008, **33**, 663; (*c*) H. Sasabe and J. Kido, *Chem. Mater.*, 2011, **23**, 621; (*d*) M. C. Gather, A. Kohnen and K. Meerholz, *Adv. Mater.*, 2011, **23**, 233; (*e*) P. Moonsin, N. Prachumrak, S. Namuangruk, S. Jungsuttiwong, T. Keawin, T. Sudyoadsuk and V. Promarak, *J. Mater. Chem. C*, 2014, **2**, 5540.

2 (*a*) B. D. Reeves, E. Unur, N. Ananthakrishnan and J. R. Reynolds, *Macromolecules*, 2007, **40**, 5344; (*b*) B. Lim, Y. C. Nah, J. T. Hwang, J. Ghim, D. Vak, J. M. Yun and D. Y. Kim, *J. Mater. Chem.*, 2009, **19**, 2380.

3 (*a*) C. Müller, S. Goffri, D. W. Breiby, J. W. Andreasen, H. D. Chanzy, R. A. J. Janssen, M. M. Nielsen, C. P. Radano, H. Sirringhaus, P. Smith and N. Stingelin-Stutzmann, *Adv. Funct. Mater.*, 2007, **17**, 2674; (*b*) G. B. Zhang, P. Li, L. X. Tang, J. X. Ma, X. H. Wang, H. B. Lu, B. S. Kang, K. W. Cho and L. Z. Qiu, *Chem. Commun.*, 2014, **50**, 3180.

4 (*a*) M. C. Scharber, D. Mühlbacher, M. Koppe, P. Denk, C. Waldauf, A. J. Heeger and C. J. Brabec, *Adv. Mater.*, 2006, **18**, 789; (*b*) J. Jo, D. Vak, Y. Y. Noh, S. S. Kim, B. Lim and D. Y. Kim, *J. Mater. Chem.*, 2008, **18**, 654; (*c*) J. R. Hollis, W. C. Tsoi and J. S. Kim, *J. Mater. Chem. C*, 2013, **1**, 6235.

5 (*a*) D. Vak, C. Chun, C. L. Lee, J. J. Kim and D. Y. Kim, *J. Mater. Chem.*, 2004, **14**, 1342; (*b*) F. Kessler, Y. Watanabe, H. Sasabe, H. Katagiri, M. K. Nazeeruddin, M. Grätzel and J. Kido, *J. Mater. Chem. C*, 2013, **1**, 107; (*c*) S. Y. Chen, J. B. Wei, K. Wang, C. G. Wang, D. Chen, Y. Liu and Y. Wang, *J. Mater. Chem. C*, 2013, **1**, 6594.

6 (*a*) M. Strukelj, F. Papadimitrakopoulos, T. M. Miller and L. J. Rothberg, *Science*, 1995, **267**, 1969; (*b*) S. Reineke, F. Lindner, G. Schwartz, N. Seidler, K. Walzer, B. Lussem and K. Leo, *Nature*, 2009, **459**, 234; (*c*) Z. W. Zheng, Q. C. Dong, L. Gou, J. H. Su and J. H. Huang, *J. Mater. Chem. C*, 2014, **2**, 9858.

7 (*a*) G. H. wang and F. Jonas, *Adv. Mater.*, 1992, **4**, 116; (*b*) M. Granstrom, M. Berggren and O. Inganas, *Science*, 1995, **267**, 1479; (*c*) P. K. H. Ho, J. S. Kim, J. H. Burroughes, H. Becker, S. F. Y. Li, T. M. Brown, F. Cacialli and R. H. Friend, *Nature*, 2000, **404**, 481; (*d*) Q. Xu, J. Ouyang, Y. Yang, T. Ito and J. Kido, *Appl. Phys. Lett.*, 2003, **83**, 4695.

8 M. Schaer, F. Nüesch, D. Berner, W. Leo and L. Zuppiroli, *Adv. Funct. Mater.*, 2001, **11**, 116.

9 M. P. de Jong, L. J. IJzendoorn and M. J. A. de Voigt, *Appl. Phys. Lett.*, 2000, **77**, 2255.

10 J. S. Kim, R. H. Friend, I. Grizzi and J. H. Burroughes, *Appl. Phys. Lett.*, 2005, **87**, 023506.

11 L. B. Groenendaal, F. Jonas, D. Freitag, H. Pielartzik and J. R. Reynolds, *Adv. Mater.*, 2000, **12**, 481.

12 S. Inaoka, D. B. Roitman and R. C. Advincula, *Chem. Mater.*, 2005, **17**, 6781.

13 (*a*) S. Miyanishi, K. Tajima and K. Hashimoto, *Macromolecules*, 2009, **42**, 1610; (*b*) Y. Lv, L. Yao, C. Gu, Y. X. Xu, Y. N. Zhang, Z. Q. Xie, L. L. Liua and Y. G. Ma, *Polym. Chem.*, 2013, **4**, 2090; (*c*) F. Huang, Y. J. Cheng, Y. Zhang, M. S. Liu and A. K. Y. Jen, *J. Mater. Chem.*, 2008, **18**, 4495.

14 M. Drees, H. Hoppe, C. Winder, H. Neugebauer, N. S. Sariciftci, W. Schwinger, F. Schaffler, C. Topf, M. C. Scharber, Z. G. Zhu and R. Gaudiana, *J. Mater. Chem.*, 2005, **15**, 5158.

15 (*a*) B. G. Kang, H. K. Kang, N. G. Kang, C. L. Lee, K. H. Lee and J. S. Lee, *Polym. Chem.*, 2013, **4**, 969; (*b*) C. Y. Lin, Y. C. Lin, W. Y. Hung, K. T. Wong, R. C. Kwong, S. C. Xia, Y. H. Chen and C. I. Wu, *J. Mater. Chem.*, 2009, **19**, 3618.

16 N. Du, M. M. D. Cin, I. Pinnau, A. Nicalek, G. P. Robertson and M. D. Guiver, *Macromol. Rapid Commun.*, 2011, **32**, 631.

17 (*a*) Y. D. Zhang, R. D. Hreha, G. E. Jabbour, B. Kippelen, N. Peyghambarian and S. R. Marder, *J. Mater. Chem.*, 2002, **12**, 1703; (*b*) G. Liaptsis and K. Meerholz, *Adv. Funct. Mater.*, 2013, **23**, 359; (*c*) J. W. Lee, H. Han, J. M. Lee, S. C. Yoon and C. J. Lee, *J. Mater. Chem. C*, 2014, **2**, 1474; (*d*) B. J. Kim, Y. Miyamoto, B. W. Ma and J. M. J. Fréchet, *Adv. Funct. Mater.*, 2009, **19**, 2273.

18 (*a*) S. Liu, X. Z. Jiang, H. Ma, M. S. Liu and A. K. Y. Jen, *Macromolecules*, 2000, **33**, 3514; (*b*) Y. Shao, X. Gong, A. J. Heeger, M. Liu and A. K. Y. Jen, *Adv. Mater.*, 2009, **21**, 1972.

19 Y. L. Chu, C. C. Cheng, Y. C. Yen and F. C. Chang, *Adv. Mater.*, 2012, **24**, 1894.

20 Q. Chen and B. H. Han, *J. Polym. Sci., Part A: Polym. Chem.*, 2009, **11**, 2948.

21 C. Weder, *Chem. Commun.*, 2005, 5378.

22 (*a*) R. Q. Png, P. J. Chia, J. C. Tang, B. L. S. Sivaramakrishnan, M. Zhou, S. H. Khong, H. S. O. Chan, J. H. Burroughes, L. L. Chua, R. H. Friend and P. K. H. Ho, *Nat. Mater.*, 2010, **9**, 152; (*b*) C. Tao, M. Aljada, P. E. Shaw, K. H. Lee, H. Cavaye, M. N. Balfour, R. J. Borthwick, M. James, P. L. Burn, I. R. Gentle and P. Meredith, *Adv. Energy Mater.*, 2013, **3**, 105; (*c*) X. Chen, L. Chen and Y. W. Chen, *J. Polym. Sci., Part A: Polym. Chem.*, 2013, **51**, 4156.

23 (*a*) H. J. Kim, A. R. Han, C. H. Cho, H. B. Kang, H. H. Cho, M. Y. Lee, J. M. J. Fréchet, J. H. Oh and B. J. Kim, *Chem. Mater.*, 2012, **24**, 215; (*b*) J. H. Koh, J. K. Koh, N. G. Park and J. H. Kim, *Sol. Energy Mater. Sol. Cells*, 2010, **94**, 436; (*c*) W. H. Chen, K. L. Wang, W. Y. Hung, J. C. Jiang, D. J. Liaw, K. R. Lee, J. Y. Lai and C. L. Chen, *J. Polym. Sci., Part A: Polym. Chem.*, 2010, **48**, 4654; (*d*) N. Y. Du, M. M. Dal-Cin, I. Pinnau, A. Nicalek, G. P. Robertson and M. D. Guiver, *Macromol. Rapid Commun.*, 2011, **32**, 631.

24 (*a*) J. F. W. Keana and S. X. Cai, *J. Org. Chem.*, 1990, **55**, 3640; (*b*) M. D. Yan, S. X. Cai, J. M. N. Wybourne and J. F. W. Keana, *Bioconjugate Chem.*, 1994, **5**, 151; (*c*) Y. W. Ebright, Y. Chen, Y. G. Kim and R. H. Ebright, *Bioconjugate Chem.*, 1996, **7**, 380.

25 (*a*) O. Inganas, W. R. Salaneck, J.-E. Österholm and J. Laakso, *Synth. Met.*, 1988, **22**, 395; (*b*) K. Yoshino, S. Nakajima, D. H. Park and R. Sugimoto, *Jpn. J. Appl. Phys.*, 1988, **27**, L716.

26 (*a*) S. Brase, C. Gil, K. Knepper and V. Zimmermann, *Angew. Chem., Int. Ed.*, 2005, **44**, 5188; (*b*) R. F. Klima and A. D. Gudmundsdottir, *J. Photochem. Photobiol., A*, 2004, **162**, 239.

27 S. T. Huang, D. J. Liaw, L. G. Hsieh, C. C. Chang, M. K. Leung, K. L. Wang, W. T. Chen, K. R. Lee, J. Y. Lai, L. H. Chan and C. T. Chen, *J. Polym. Sci., Part A: Polym. Chem.*, 2009, **47**, 6231.

28 C. A. Zuniga, S. Barlow and S. R. Marder, *Chem. Mater.*, 2011, **23**, 658.

29 X. Jiang, S. Liu, M. S. Liu, P. Herguth, A. K. Y. Jen, H. Fong and M. Sarikaya, *Adv. Funct. Mater.*, 2002, **12**, 745.

30 J. W. Kang, D. S. Lee, H. D. Park, Y. S. Park, J. W. Kim, W. I. Jeong, K. M. Yoo, K. Go, S. H. Kim and J. J. Kim, *J. Mater. Chem.*, 2007, **17**, 3714.

31 Y. H. Lim, Y. S. Park, Y. R. Kang, D. Y. Jang, J. H. Kim, J. J. Kim, A. Sellinger and D. Y. Yoon, *J. Am. Chem. Soc.*, 2011, **133**, 1375.

32 (*a*) C. D. Müller, A. Falcou, N. Reckefuss, M. Rojahn, V. Wiederhirn, P. Rudati, H. Frohne, O. Nuyken, H. Becker and K. Meerholz, *Nature*, 2003, **421**, 829; (*b*) M. M. Shi, J. J. Lin, Y.-W. Shi, M. Ouyang, M. Wang and H. Z. Chen, *Mater. Chem. Phys.*, 2009, **115**, 841.